EFFECT OF FREESTREAM TURBULENCE ON THE UNSTEADY WAKE CHARACTERISTICS OF A NOTCHBACK AHMED BODY

Ashim Chhetri
Department of Mechanical, Industrial and Aerospace Engineering
Concordia University
Montreal, QC, Canada, H3G 1M8
a_chhe@live.concordia.ca

Ebenezer E. Essel
Department of Mechanical, Industrial and Aerospace Engineering
Concordia University
Montreal, QC, Canada, H3G 1M8
ebenezer.essel@concordia.ca

ABSTRACT

Time-resolved particle image velocimetry is used to investigate the effects of freestream turbulence (FST) on the unsteady wake dynamics of a notchback Ahmed body with an effective backlight angle of $\beta_e = 17.8°$. Experiments were conducted at a fixed Reynolds number based on the body height of $Re = 1.7 \times 10^4$. Elevated FST intensities of $I_u = 5\%, 10\%$ and 15%, with corresponding integral length scales of $L_u = 0.29 - 1.07H$, were generated using passive regular and fractal grids to replicate realistic on-road turbulence conditions. These test cases were compared to a baseline case of $I_u = 1.5\%$ (without grid). Mean velocity, Reynolds stresses and two-point auto-correlation are used to characterize the flow structures, while spectral proper orthogonal decomposition (SPOD) is used to study the effect of FST on coherent structures at dominant frequencies. The results show that increasing FST induces a transition from a laterally asymmetric wake to a symmetric configuration. Elevated FST also promotes earlier flow reattachment on the deck, leading to an expansion of the bubble behind the vertical back. Spectral analysis shows suppression of the shear-layer vortex shedding, with a reduction in Strouhal number of up to 44%, accompanied by synchronized low-frequency pumping motion at higher turbulence levels. Two-point autocorrelations and SPOD reveal enhanced spatial coherence and a shift toward large-scale low-frequency structures with increasing FST.

INTRODUCTION

Transportation remains a significant contributor to global greenhouse gas (GHG) emissions, accounting for approximately one-fifth of the global total. Ground vehicles contribute nearly 75% of these emissions, largely due to the impact of aerodynamic drag on fuel consumption. With the increasing global shift toward electric and hydrogen-powered vehicles, reducing drag has become a critical engineering objective to improve driving range and energy efficiency. Achieving this goal requires a fundamental understanding of vehicle flow dynamics under realistic on-road conditions, where freestream turbulence (FST) levels can vary significantly from 2% to 16% depending on traffic, terrain, and roadside obstacles. Similarly, the integral length scale (L_u), representing the size of energy-containing eddies, can range from $0.3H$ to $3.5H$ (where H is the vehicle height) (Passaggia et al., 2021), Such variations in FST fundamentally modify shear-layer growth, size of recirculation bubble, and vortex shedding, thereby influencing the overall wake dynamics and aerodynamic drag.

To investigate the wake characteristics while avoiding the design complexities of ground vehicles, generic models such as the Windsor body, DrivAer model, and Ahmed body are used as baseline case. The notchback Ahmed body, representing sedan-type geometries, exhibits complex wake dynamics compared to square-back repersenting truck and hatchback represeting SUVs models (Sims-Williams et al., 2011; He et al., 2022). For the notchback Ahmedbody, the separated flow from the roof may either reattach on the deck or continue downstream into the wake, which depends on vehicle geometry and flow conditions such as backlight angle (β) and effective backlight angle (β_e) (Sims-Williams et al., 2011), roof trailing edge roundness (He et al., 2021a) and Reynolds number (He et al., 2022; Ouedraogo & Essel, 2024). Previous studies have identified two primary regimes based on β_e: reattached flow ($\beta_e < 25.3°$) and fully separated flow ($\beta_e \geq 25.3°$). Within the reattached regime, the wake can alternate between symmetric attachment of flow on the deck (figure 1a) and asymmetric attachment (figure 1b). The instabilities in the shear layers can also trigger stochastic switching, producing dynamic modes such as bi-stablity and tri-stablity under zero yaw (He et al., 2022). While previous studies have demonstrated sensitivity of notchback wake to geometric and Reynolds number effects, they have mostly been conducted under low freestream turbulence intensities of less than $I_u = u_{rms}/U_\infty = 1\%$ (where u_{rms} is root mean square of the streamwise velocity fluctuation), which do not reflect realistic on-road turbulence levels.

Studies on square-back and hatchback Ahmed bodies have shown that increasing FST significantly modifies wake dynamics, leading to a reduction in the wake recirculation

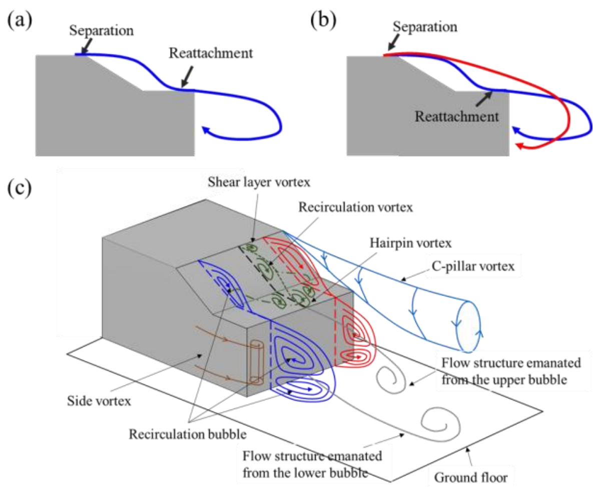

Figure 1. Sketch of the streamlines describing the flow regime: (a) Symmetric flow; (b) Asymmetric flow; (c) Flow structure around the notchback Ahmed body with $\beta = 25°$ (He et al., 2022)

bubble, suppression of dominant vortex shedding frequencies, and an increase in bi-stability switching rates (Cadot et al., 2020; Chen et al., 2023). For square-back configurations, the increase in the switching rate with increasing FST is attributed to enhanced shear-layer entrainment that thickens vorticity and destabilizes the toroidal recirculation region, thereby promoting the shedding of large-scale vortices that trigger state reversals. Chen et al. (2023) employed improved delayed detached eddy simulation (IDDES) to study square-back Ahmed body under varying FST levels ($I_u = 3.4\% - 11.4\%$ and $L_u/H = 0.24 - 0.21$). They found that increasing FST enhances entrainment of the oncoming flow into the wake, promotes shear layer thickening, and shortens the wake recirculation bubble. Similarly, for hatchback, increased FST strengthens the spatial and temporal coupling between the C-pillar vortices and the shear layer separated from the slant. This reinforced interaction energizes the flow structures over slanted surface, making the wake more susceptible to perturbations that drive bi-stable switching (Sagharichi and Tachie, 2025). In contrast to the square-back and hatchback, the influence of FST on the flow dynamics of the notchback Ahmed body has not been investigated in the open literature, and therefore, is not well understood. Consequently, the mechanisms governing the unsteady wake behavior, including the possible occurrence and modulation of bi-stability under elevated FST conditions, remain unknown. Understanding these dynamics can contribute to the development of effective flow control strategies for energy-efficient vehicles under realistic on-road conditions.

Therefore, the objective of the present study is to investigate the effects of FST on the unsteady wake dynamics of a notchback Ahmed body with $\beta_e = 17.8°$. Time-resolved particle image velocimetry (TR-PIV) measurements were performed at a fixed Reynolds number ($Re = 1.7 \times 10^4$) for turbulence intensities of $I_u = 5\%$, 10% and 15%, corresponding to integral length scales $L_u/H = 0.29$ - 1.07, generated by passive regular and fractal grids. These cases are compared against a baseline low-turbulence case of $I_u = 1.5\%$.

EXPERIMENTAL SETUP & PROCEDURE

Test facility and test model

The experiments were performed in an open recirculating water channel facility equipped with a time-resolved particle image velocimetry (TR-PIV) system at the University of Manitoba. The flow was driven by a 30 kW variable-speed pump through a flow conditioning unit and a 4.88: 1 contraction before entering the transparent acrylic test section of 6.00 m × 0.60 m × 0.45 m (length × width × depth).

Figure 2 shows a schematic drawing of the 1: 4 scaled notchback Ahmed body and the adopted Cartesian coordinate system. The model has a height $H = 72$ mm, length $L = 3.82H$, width $W = 1.35H$, deck length $L_D = 0.469$H, deck height $H_D = 0.68H$, backlight angle $\beta = 30°$, and effective backlight angle $\beta_e = 17.8°$.

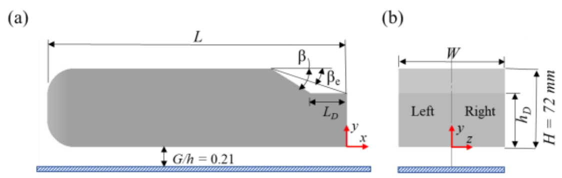

Figure 2. Schematic of he notchback Ahmed body with the nomenclature used in the present study.

Table 1. Summary of the approach flow condition.

Cases	u_{rms}/v_{rms}	$I_u(\%)$	L_u/H	x_{GL}/H
Base	1.10	1.5	–	–
R-5	1.13	5.0	0.68	19.16
R-10	1.09	10.0	0.29	3.88
F-10	1.16	10.0	1.07	17.91
F-15	1.14	15.0	1.00	16.52

The Ahmed body was mounted on a raised plate with a length of $42H$ that spanned the test section width and positioned 50 mm above the floor to minimize channel boundary layer effect on the wake dynamics. The water depth in the test section was maintained at $5.22H$ above the raised plate. The ground clearance was $G = 0.21H$ and the boundary layer thickness at model's leading edge was $0.63H$. The freestream velocity was $U_\infty = 0.24$ ms^{-1} and the Reynolds number based on the body height ($Re = U_\infty H/\nu$) was 1.7×10^4. The turbulence intensity measured along the centerline of the channel, without any turbulence grids was $I_u = 1.5\%$.

Turbulence Generation

Elevated FST was generated using two passive grids: regular grid (R) and fractal grid (F) made of stainless steel, positioned at the inlet of the test section. The geometric specifications of these grids are similar to those reported in Sagharichi and Tachie (2025). The turbulence intensities of $I_u = 5\%$ and 15% were generated using a regular grid (R-5) and a fractal grid (F-15), and the corresponding integral length scales were $L_u/H = 0.68$ and $1.00H$, respectively. Measurements were also conducted for $I_u = 10\%$ generated from a regular grid (R-10) and a fractal grid (F-10) to induce different length scales, i.e., $L_u/H = 0.29$ and $L_u/H = 1.07$, respectively. The production and decay of turbulence downstream of the grids were characterized prior to installing the Ahmed body. The distance between the raise plate and the grids (x_{GL}) was varied to ensure the leading edge of the Ahmed body was positioned within the decay region, where the flow is homogeneous and isotropic. Details of the grid characterization are reported in Sagharichi and Tachie (2025). Here, these grid turbulence cases were compared against the reference case ($I_u = 1.5\%$), as summarized in Table 1.

PIV measurements

The velocity fields were measured using a planar TR-PIV system. The flow was seeded with 10 μm silver-coated hollow glass spheres of a specific gravity of 1.4. Two high-speed 12-bit CMOS cameras with a resolution of 2560×1600 pixels, were used to capture instantaneous images of the flow illuminated with a dual-cavity high-speed pulsed Nd:YLF laser. For each test case, measurements were performed in the vertical symmetry plane ($x - y, z/d = 0$) of the Ahmed body, with combined field of views (FOV1 and FOV2) denoted as V1 to characterize the wake dynamics. To investigate the wake asymmetry and associated instabilities, measurements were also performed in the horizontal plane ($x - z, y/H = 0.84$) at the mid-height of slant of the Ahmed body, with field of view (FOV3) denotes as H1. The magnification factor of each FOV was 8.89 pixel/mm in the $x - y$ plane and 9.25 pixel/mm in the $x - z$ plane. A schematic of the PIV setup is provided in figure 3. Based on a

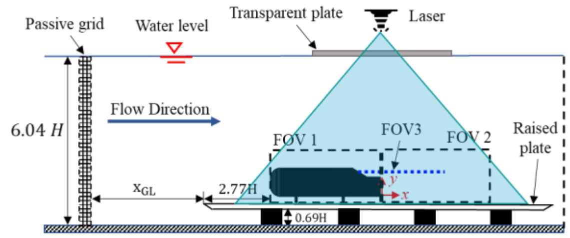

Figure 3. Schematic of the experimental setup with the nomenclature used in the present study.

convergence test, a sample size of 60,000 instantaneous images was acquired for each measurement plane at 806 Hz to resolve the spatio-temporal wake dynamics. The data was post-processed using an adaptive multi-grid cross-correlation. The initial interrogation area was set to 128×128 pixels with a 50% overlap and refined to a final interrogation window 24×24 pixels with a 75% overlap, resulting in a vector spacing of $0.009H$. The uncertainty in the mean velocities is less than 2% while the Reynolds stresses are about 10%.

RESULTS AND DISCUSSION

Mean Flow and Turbulence Statistics

Figure 4 shows contours of the wall-normal mean velocity in the vertical plane (V1) and spanwise mean velocity in the horizontal plane (H1), with the mean streamlines superimposed for the Base, R-5 and F-15 cases. In each plot, the reverse flow region ($U < 0$) is demarcated using the isopleth of $U/U_\infty = 0$. The saddle point is marked by red dot, the maximum spanwise extent (y_r) from the saddle point to the centerline is shown by

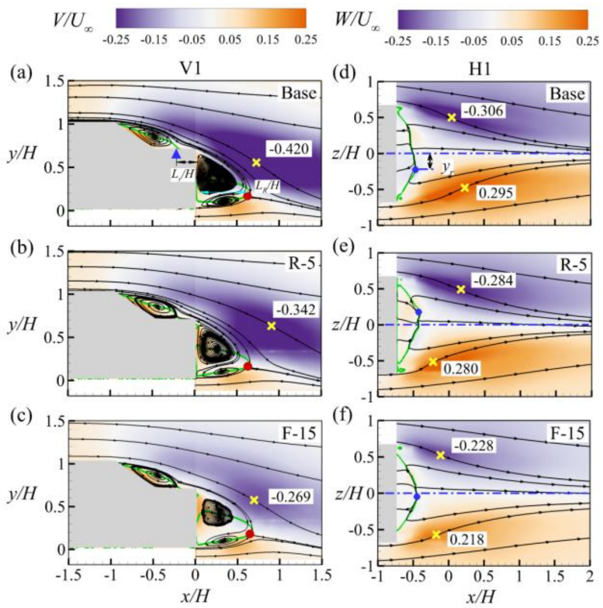

Figure 4. Contour of (a-c) wall-normal mean velocity and (d-f) spanwise mean velocity for (a,d) Base, (b,e) R-5, and (c,f) F-15 cases. Superimposed are the mean streamlines, and the isopleth of $U/U_\infty = 0$ (green line), which bounds the reverse flow areas. The maximum spanwise extent of the reverse-flow region (y_r) is marked by the blue dot, shown on H1. The saddle point is marked with the red dots, while the yellow cross marks the local peak.

the blue dot, and the cross denotes the local velocity peak. In V1, a recirculation bubble forms on the slanted surface as the separated flow from the roof trailing edge reattaches at the deck. Subsequent separation at the top and bottom trailing edges of the vertical back generates counter-rotating recirculation bubbles, associated with strong downwash (i.e., $V/U_\infty < 0$) from the roof and upwash (i.e., $V/U_\infty < 0$) from the gap between the body and the ground. The upwash and downwash meet at the saddle point, which is located closer to the bottom wall for a dominant downwash flow and farther away from the wall for a dominant upwash flow. The effect of FST on the mean recirculaton bubbles over slant and behind back are charaterized using reattachment length, L_r/H (streamwise distance from reattachment point on the deck to the trailing edge of the deck) and recirculation length and L_R/H (streamwise distance from the back to the furthest location of the contour line of $U/U_\infty = 0$). For the Base case, V1 exhibits $L_r/H = 0.205$ and $L_R/H = 0.651$. With increasing turbulence intensity, the L_r/H increases to 0.215 for R-5 and 0.224 for F-15, while L_R/H increases to 0.653 and 0.667, respectively, indicating earlier reattachment on the deck and an enlargement of the bubble behind the vertical back. This behavior is attributed to enhanced flow entrainment and mixing with increasing turbulence, which promotes the earlier recovery of surface pressure by drawing higher-momentum fluid into the recirculation region leading to early reattachment. The peak downwash velocity decreases from -0.420 in the Base to -0.342 in R-5 and -0.269 in F-15, which causes the saddle point of the bubble behind the back to shift upwards. In H1, the spanwise entrainment of flow increases on one side, contributing to wake asymmetry in the Base and R-5 cases. As FST increases, $|y_r|$ decreases from 0.233 for the Base to 0.177 for R-5 and 0.036 for F-15, and the recirculation bubble approaches a symmetric distribution. The effect of turbulence length scale was examined by comparing the R-10 and F-10 cases (figure not shown for brevity). While both cases exhibit a symmetric wake, increase in length scale reduces the peak spanwise velocity. These results indicate that an increase in FST reduces lateral asymmetry, enhances reattachment on the deck, elongates the back recirculation bubble, and reduces downwash.

The contours of turbulent kinetic energy (TKE) is shown in figure 5. The TKE was determined based on the measured streamwise, $\langle u'u' \rangle$ and wall-normal, $\langle v'v' \rangle$ Reynolds normal stresses in V1 as $TKE = 0.5(\langle u'u' \rangle + \langle v'v' \rangle)$, and in H1 plane, measured based on streamwise and spanwise, $\langle w'w' \rangle$ Reynolds normal stresses as $TKE = 0.5(\langle u'u' \rangle + \langle w'w' \rangle)$. The turbulent kinetic energy is enhanced along the mean shear layer bounding the reverse flow region. In V1, the Base exhibits intense peak region of 0.062 over the slant and 0.051 behind the back. Increasing FST reduces the peak by up to 19% for R-5 and 11% for F-15 over the slant and by 14% for R-5 and 35% for F-15 behind the back. This suppression of peak TKE aligns with findings in hatchback models where higher FST intensity disrupt the formation of strong coherent structures while shifting energy to low-frequency motions (Sagharichi and Tachie, 2025). In H1, the TKE is more pronounced in the left side ($z/H < 0$) of the body, which signifies a higher shedding dynamics at this halves. The increase in I_u enhances the peak TKE while the length scales reduces the peak (figure not shown for brevity). Further analysis of the Reynolds normal stresses contributing to the TKE reveals that the asymmetry is most pronounced in $\langle u'u' \rangle$(the dominant component), compared with $\langle v'v' \rangle$ and $\langle w'w' \rangle$.

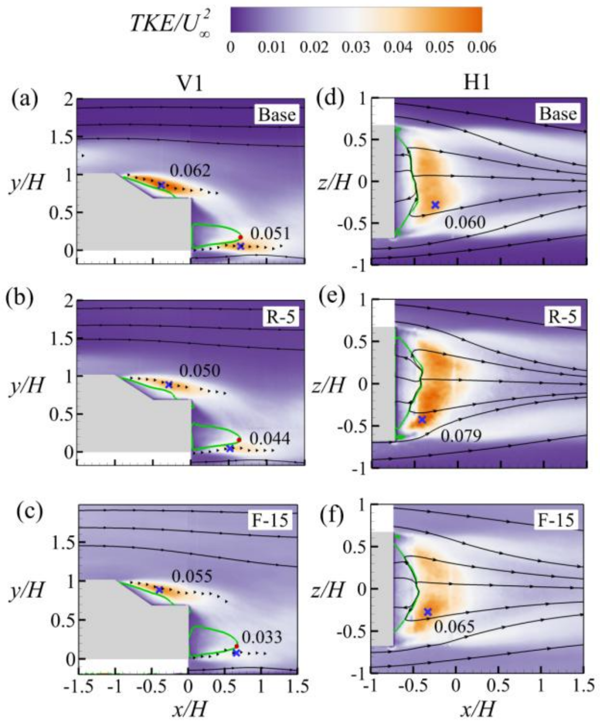

Figure 5. Contours of normalized TKE superimposed with mean streamlines for (a,d) Base, (b,e) R-5, and (c,f) F-15 cases. The green line represents the isopleth $U/U_\infty = 0$ which bounds the reverse flow region. The black dots in V1 marks the trajectory of maximum TKE. The blue cross marks the local maxima and red dot represents the saddle point.

Spatial coherence of flow structures

To understand the influence of FST on the large-scale structures, the spatial coherence is examined along the mean shear layer in H1, using two-point autocorrelations of the streamwise velocity fluctuations evaluated as

$$R_{u'u'}(x^*, w^*) = \frac{\langle u'(x_{ref}, w_{ref}) u'(x^*, w^*) \rangle}{\langle \sqrt{u'^2}(x_{ref}, w_{ref}) \sqrt{u'^2}(x^*, w^*) \rangle} \quad (1)$$

where (x_{ref}, y_{ref}) denotes the reference location, and $(x^*, w^*) = (x_{ref} + \Delta x, w_{ref} + \Delta w)$ represents a spatially offset location, with Δx and Δy being the separation in the streamwise and spanwise directions, respectively. Figure 6 shows contours

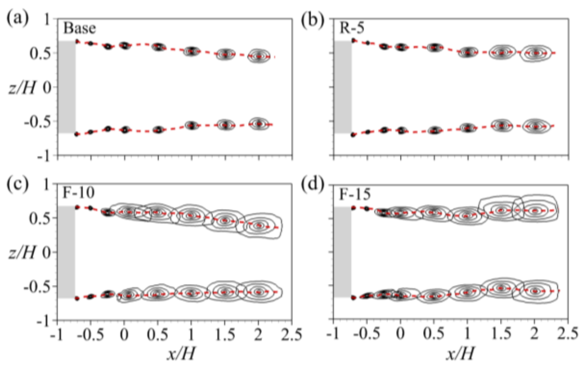

Figure 6. Contours of the R_{uu} distribution along the mean shear layer in H1. Contour levels at intervals of 0.1 are from 0.5 to 1.

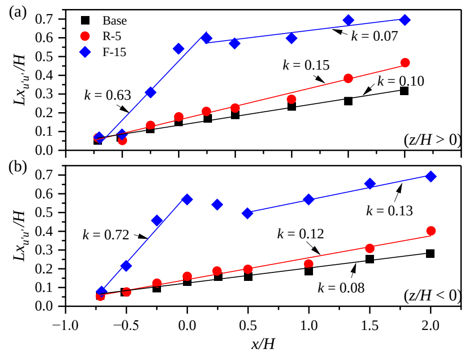

Figure 7. Contours of the $R_{u'u'}$ distribution along the (a) right $(z/H > 0)$ and (b) left $(z/H < 0)$ mean shear layer in H1. Contour levels at intervals of 0.1 are from 0.5 to 1.

of the two-point correlations of $R_{u'u'}$, which exhibts the growth of vortex along the mean shear line. The contour ranges from 0.5 to 1, at an interval of 0.1. With increasing FST, the correlated region stretches significantly, indicating enhanced vortex generation and subsequent merging, which promotes the formation of larger spatially coherent structures in the wake. To further characterize the spatial structures, the distribution of streamwise extent of $R_{u'u'}$, defined as twice the streamwise distance from the self-correlation point to the farthest downstream point on the 0.5 isopleth is plotted along the right $(z/H > 0)$ and left mean $(z/H < 0)$ shear layer in H1, as shown in figure 7. A least-squares line is fitted to each profile to determine the growth rate, $k = Lx_{u'u'}/dx$. For the Base and R-5, a higher growth rate of $k = 0.13 \pm 0.02$ is observed at the right side compared to the left with $k = 0.10 \pm 0.02$, while for F-15 the left exhibits a larger structure with $k = 0.72$ compared to the right side of $k = 0.63$. The significant increase in k for F-15 is attributed to the use of fractal grids that generates eddies of large length scale which contributes to the enhanced coherent structures.

Spectral Analysis

The vortex shedding characteristics in the vertical and horizontal planes are investigated using the pre-multiplied frequency spectra of streamwise velocity fluctuations, shown in figure 8. The spectra were extracted at the location of maximum root mean-square of the streamwise velocity fluctuations (u_{rms}) behind the slant for each case. In the vertical plane (V1), the dominant Strouhal number $(St_H = fH/U_\infty)$ is 0.738 for Base, associated with shear layer vortex shedding. With increasing turbulence intensity, the dominant St_H decreases by 36% for R-5 (0.472) and by 44% for F-15 (0.413), indicating suppression of the primary shedding mode. The reduction in Strouhal number with increase freestream turbulence intensity is consistent with previous studies by Cadot et al. (2020) for square-back Ahmed body and Sagharichi and Tachie (2025) for hatchback Ahmed body. In horizontal plane (H1), the Base case exhibits a dominant frequency of $St_H = 0.531$, associated with shear - layer shedding from the upper slant (He et al., 2021b). With increasing FST, this dominant shedding frequency increases by 11% for R-5 (0.590) and by 22% for F-15 (0.649). Furthermore, the frequency signature of the horizontal plane for Base $(St_H = 0.531)$ and R-5 $(St_H = 0.177)$ are also present in the vertical plane, indicating the strong influence of the spanwise vortex structures. However, with increasing turbulence intensity,

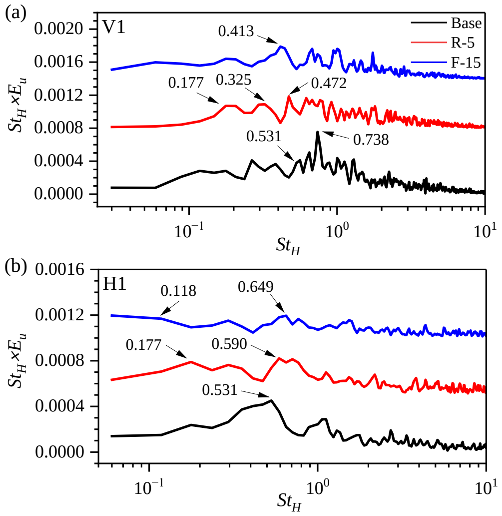

Figure 8. Pre-multiplied frequency spectra of the streamwise velocity fluctuations in (a) V1 and (b) H1, measured at peak u_{rms} location over the slant for Base, R-5 and F-15. For clarity, the spectra are offset arbitrarily.

the shedding dynamics become more anisotropic. The shedding frequency also decreases with increasing length scale from $St_H = 1.063$ for R-10 to $St_H = 0.531$ for F-10.

The dominant frequencies associated with the pumping motion of the reverse flow regions over the slant are examined using pre-multiplied spectra of the reverse flow area fluctuations, shown in figure 9. The Base case exhibits a low-frequency pumping motion, $St_p = f_p H/U_\infty$ of 0.089 in V1 and 0.103 in H1 along with accompanying harmonics. The disparity in the pumping frequency is attributed to the asymmetry of the wake. The frequency reduces for R-5 to 0.059 in V1 and 0.089 in H1. Moreover, for R-5 in V1, the dominant frequency 0.325 is similar to the shear layer vortex frequency (figure 8),

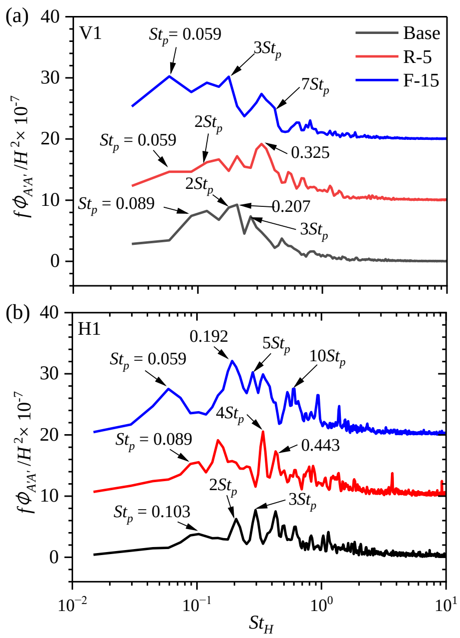

Figure 9. Pre-multiplied frequency spectra of the fluctuations of the reverse flow area for Base, R-5 and F-15. The spectra are offset arbitrarily for clarity.

indicating a strong influence of shear layer vortex shedding on the pumping motion. For F-15, a synchronized low pumping frequency of 0.059 is observed in both planes attributed to symmetric wake over the slant.

Spectral Proper Orthogonal Decomposition

The spatio-temporal characteristics of the vortical structures associated with the dominant frequencies are examined using spectral proper orthogonal decomposition (SPOD). The SPOD method extract the spatial energetic structures of the entire frequency domain and sort these structures based on their advection frequency. Following Towne et al. (2018), the SPOD procedure involves performing a Fourier transform of the time-resolved flow field and decomposing the transformed flow field into different mode using the POD technique. The fluctuating velocity component is then expressed as

$$\vartheta'(x,y,t) = \sum_{j=1}^{\infty}\sum_{m=1}^{\infty} \phi_j^m(x,y) a_j^m e^{-i\omega_j t} + c.c. \qquad (3.4)$$

where the indices j and m represent the frequency and mode number, respectively. The term ϕ_j^m refers to the orthogonal set of spatial eigenfunctions (modes) and a_j^m their associated coefficients. The wavenumber is given by $\omega_j = 2\pi f_j$, where $i = \sqrt{-1}$ and $c.c.$ denotes the complex conjugate.

The pre-multiplied energy spectra of the most energetic mode, Mode 1 for V1 and H1 are shown in figure 10. The dominant frequencies decrease with increase in turbulence intensity in V1, from $St_H = 0.767$ for the Base to 0.443 for R-5 and 0.118 for F-15, and in H1, from $St_H = 0.413$ for the Base to 0.177 for R-5 and 0.148 for F-15. In V1, similar Strouhal numbers were also observed in spectra of velocity fluctuations for the Base and R-5, corresponding to the shear layer vortex shedding frequency. While for F-15, the dominant peak in V1 ($St_H = 0.118$) corresponds to the second harmonic of the pumping motion (figure 9a). This indicates that increasing FST results in the dominance of low frequency pumping motion in the wake, suppressing the higher frequency shear layer vortex shedding. With increasing length scale, the dominant frequency decreases from $St_H = 0.531$ for R-10 to 0.354 for F-10 in H1. Similar to V1, SPOD spectra of H1 also reveals the suppression

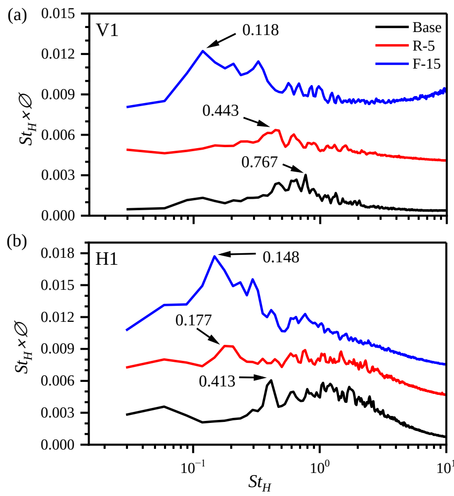

Figure 10. Premultiplied energy spectra of SPOD Mode 1 at the dominant Strouhal numbers for each test case.

of high-frequency modes and shift toward lower frequencies with increasing FST, indicating a redistribution of energy from small-scale instabilities to larger, low-frequency structures (Chen et al., 2023; Sagharichi and Tachie, 2025).

Contours of the streamwise component ϕ_u of Mode 1 at the dominant Strouhal number for Base, R-5 and F-15 are shown in figure 11. In V1, for the Base case, alternating vortices are generated at the roof that bend toward the deck under the influence of downwash, which deflects the structures further toward the wall as it evolves downstream and merges with the structures associated with the upwash motion from the underbody flow. The structures are more spatially distributed for R-5. While for F-15, the low-momentum region within the reverse flow over the slant gradually expands until it collapses, resulting in shedding downstream. In H1 plane, a complex interaction between the low and high momentum regions is observed around the reverse flow region and along the mean shear line. For the Base case, an alternating vortices are generated along the centerline surrounded by shedding of structures with opposite signs representing hair-pin vortices. For R-5, the low and high momentum packects are observed on the either side. These packets spread over a wider region for F-15. The dominance of these large-scale structure exhibited in both planes may account for wake symmetry as turbulence increases.

CONCLUSION

A time-resolved PIV system was used to investigate the effect of freestream turbulence intensity (FST) on the unsteady wake characteristics of a notchback Ahmed body with an effective backlight angle of $\beta_e = 17.8°$. Three turbulence intensities of $I_u = 5\%$, 10% and 15%, corresponding to integral length scales $L_u/H = 0.29$ - 1.07, were generated using passive regular and fractal grids to mimic the realistic on-road turbulence levels. These cases are compared against a baseline low-turbulence case of $I_u = 1.5\%$.

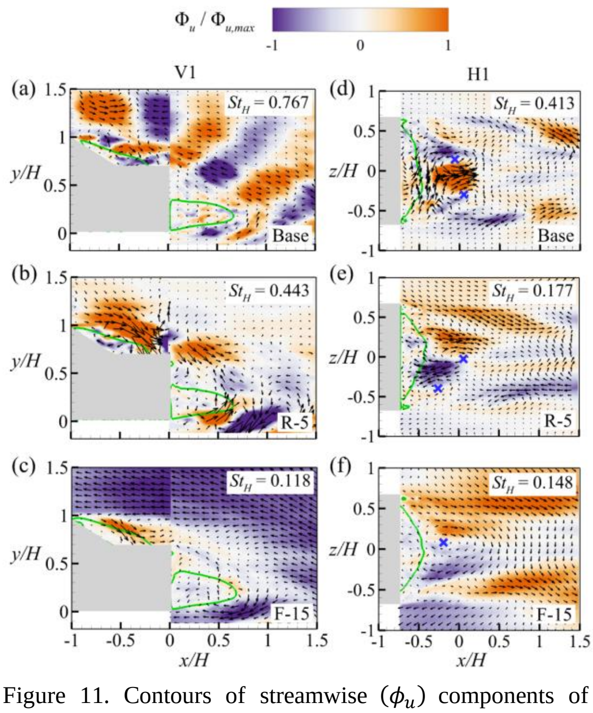

Figure 11. Contours of streamwise (ϕ_u) components of Mode 1 at the dominant Strouhal numbers for (a,d) Base, (b,e) R-5, and (c,f) F-15 cases. The vectors of ϕ_u and ϕ_w are shown on each plot.

The results showed that increasing FST induces a transition from a laterally asymmetric wake to a symmetric wake. Elevated FST promotes earlier reattachment on the deck, leading to an expansion of the recirculation bubble behind the vertical back. These effects are attributed to the evolution of coherent structures in the wake, where higher FST enhances spatial coherence the organized structures.

Furthermore, elevated FST suppresses shear layer vortex shedding, with the dominant Strouhal number decreasing by 44% in the F-15 case. In addition, a synchronized low-frequency pumping motion ($St_p = 0.059$) is observed in both vertical and horizontal planes. SPOD analysis reveals that increasing FST suppresses high-frequency modes and shifts energy toward lower frequencies structures, promoting symmetric wake. These findings highlight that, under realistic on-road turbulence, the unsteady wake of a notchback vehicle is predominantly governed by low-frequency coherent motions, an important consideration for designing flow-control strategies and improving aerodynamic efficiency in ground vehicles.

REFERENCES

Cadot, O., Almarzooqi, M., Legeai, A., Parezanovic, V., and Pastur, L., 2020, “On three-dimensional bluff body wake symmetry breaking with freestream turbulence and residual asymmetry,” *Comptes Rendus Mécanique*, Vol. 348, pp. 509–517.

Chen, G., Li, X. B., He, K., Cheng, Z., Zhou, D., and Liang, X. F., 2023, “Effect of the free-stream turbulence on the bi-modal wake dynamics of square-back bluff body,” *Physics of Fluids*, Vol. 35, 015158.

He, K., Minelli, G., Su, X., Gao, G., and Krajnović, S., 2021a, “Influence of the rounded rear edge on wake bi-stability of a notchback bluff body,” *Physics of Fluids*, Vol. 33, 115107.

He, K., Minelli, G., Wang, J., Dong, T., Gao, G., & Krajnović, S. (2021b). Numerical investigation of the wake bi-stability behind a notchback Ahmed body. Journal of Fluid Mechanics, 926, 1–29.

He, K., Minelli, G., Su, X., Gao, G., and Krajnović, S., 2022, “On state instability of the bi-stable flow past a notchback bluff body,” *Journal of Fluid Mechanics*, Vol. 931, R6.

Ouedraogo, N. F., and Essel, E. E., 2024, “Effects of Reynolds number on the wake characteristics of a notchback Ahmed body,” *Journal of Fluids Engineering*, Vol. 146, 111302.

Passaggia, P. Y., Mazellier, N., and Kourta, A., 2021, “Aerodynamic drag modification induced by free-stream turbulence effects on a simplified road vehicle,” *Physics of Fluids*, Vol. 33, 105108.

Sagharichi, A., and Tachie, M. F., 2025, “Effects of freestream turbulence intensity on flow dynamics and vortical structures around a high-drag Ahmed body,” *Physics of Fluids*, Vol. 37, 075108.

Sims-Williams, D., Marwood, D., and Sprot, A., 2011, “Links between notchback geometry, aerodynamic drag, flow asymmetry and unsteady wake structure,” *SAE International Journal of Passenger Cars – Mechanical Systems*, Vol. 4, pp. 156–165.

Towne, A., Schmidt, O. T., and Colonius, T., 2018, “Spectral proper orthogonal decomposition and its relationship to dynamic mode decomposition and resolvent analysis,” *Journal of Fluid Mechanics*, Vol. 847, pp. 821–867.